WHAT AFFECTS THE FREEZING BEHAVIORS OF CEMENT-BASED POROUS MATERIALS: THE ROLE OF THE UNFROZEN LIQUID-LIKE LAYER

Q. Zeng [1] and S.L. Xu[1]
[1] Institute of advanced engineering structures and materials,
College of civil engineering and architecture,
Zhejiang University, Hangzhou, P.R. China.
Email:cengq14@zju.edu.cn

ABSTRACT

A key factor that affects freeze-thaw damages of cement-based porous materials (CBPMs) is the amount of the freezable water confined in the pores that generate large internal pressures during freezing. Taking account of an unfrozen liquid-like layer (ULLL) between ice crystals and pore wall, this paper investigates deformations of a saturated CBPM specimen under freezing with different thickness values of the ULLL. To bridge the macro strains and the local pressure exerted on the pore wall of the material, the thermodynamic equilibrium between the water and ice, and a poroelastic approach were adopted. The hydraulic pressure by volume change as phase transition takes place in the pores, the fusion pressure by energy change as ice forms and penetrates through the thin pores and the hydrothermal pressure by TEC discrepancies between the pore fluids and solid substrate dominate the internal freezing stress. The obtained results reveal that the ULLL plays an important role on the estimation of the amount of ice crystals confined in the pores, and thus influences the pore pressures and deformations of the CBPM specimen used. Appropriate model of the ULLL helps to decrease the deviations between the predicted strains and the experimental data.

KEYWORDS

Freeze-thaw, unfrozen liquid-like layer, pore pressure, poroelasticity.

INTRODUCTION

Frost damage remains the utmost durability problem for cement-based porous materials (CBPMs). Numerous studies have been conducted on the relevant issues (Coussy 2005, Coussy and Monteiro 2008, Dai *et al*. 2013 Scherer 1999, Scherer and Valenza 2005, Wang *et al*. 2014, Sun and Scherer 2010a, Zeng *et al*. 2011,2013a,2014a,b), but more and more experimental and theoretical findings indicated that the mechanical behaviors of CBPMs, together with the chemical--physical process of water solidification confined in the thin pores and the influence factors, need to be advanced.

The material damages relate closely to the mechanical effects arising from the liquid/ice phase change in the porous network. Previous poromechanical studies (Coussy 2005,Coussy and Monteiro 2008, Sun and Scherer 2010a) have linked the internal freezing deformation of a liquid-saturated porous medium to the density change, interface energy, fusion entropy, and thermal expansion coefficient (TEC) discrepancy between pore fluids and solid phases. However, the modeled pore pressures arise easily to 100 MPa at -20 ℃ (Coussy and Monteiro 2008) and the freezing strains can be up to the magnitude of 1% (Coussy 2005, Fabbri *et al*. 2013), which are dramatically larger than the observed data both in-situ and in laboratory. In these poromechanical-based works on the freezing behaviors of CBPMs, the effect of an unfrozen liquid-like layer (ULLL) between ice crystals and pore wall has not been taken into account. Recent experimental and modeling investigations (Zeng *et al*. 2011, 2013a, 2014a,b) have evidenced that the poroelastic model with a ULLL correction can capture the strains of CBPMs saturated with water and/or NaCl solution to a certain degree. However, how and to what extent the thickness of ULLL affecting the freezing behaviors of CBPMs have not been addressed. Motivated by this need, five different models (values) of the thickness of ULLL are adopted in this study. By using the poroelastic approach with the ULLL models, the ice volume distribution (IVD) and water saturation degree of a hardened cement paste (HCP) specimen are estimated. The consequential freezing pressures and strains are analyzed and discussed. The results help to clarify the roles of the ULLL between ice crystals and pore wall to the freezing behaviors of CBPMs.

CONFINED FREEZING

Freezing of water confined in thin space is different with that of bulk water. The premise of ice formation in both manners, however, is that the chemical potential of ice crystals is equal to or lower than that of liquid water. Due to the curvature effect of pores, freezing temperature is depressed because of the lower chemical potential of the confined water. Generally, freezing first takes place in large pores, then penetrate into thinner pores as temperature decreases (Scherer 1999). Triggered by the crystal/liquid interfacial energy (γ_{cl}) and the anisotropic pore geometry (curvature effect), crystallization in confined space generates crystallization pressure (P_A) on the pore wall. Figure 1 exemplifies a case of crystallization pressure building up when ice is entrapped in an anisotropic pore with a large pore chamber connected with small entries. The differences of curvatures of crystal sides (κ_{cl}^s) and crystal caps around pore entries (κ_{cl}^e) generate the crystallization pressure, i.e., $P_A = \gamma_{cl}\left(\kappa_{cl}^e - \kappa_{cl}^s\right)$ (Scherer 1999, Scherer and Valenza 2005). The crystallization pressure is not uniform for an ice crystal. When pore side has a relatively flat curve (point P in Fig. 1), the generated crystallization pressure is relative high. At point N the curvature is negative, crystallization pressure is thus enhanced. Similar cases can be found elsewhere (Dai et al. 2013, Zeng et al. 2014a, Scherer and Valenza 2005).

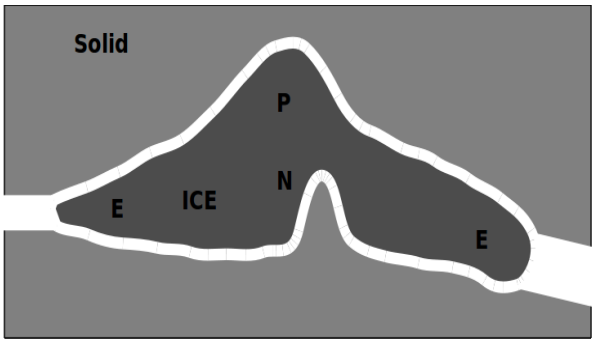

Figure 1 Schematic illustration of an ice crystal in big pore chamber with small entries, see also (Scherer and Valenza 2005, Dai *et al*. 2013, Zeng *et al*. 2014a).

The crystallization pressure, however, remains difficult to be estimated because of the anisotropy and complexity of the pores of CBPM (Zeng *et al*. 2012). Based on the thermodynamic equation for the energy balance at the interfaces of ice crystals and pore water, however, one can easily obtain the pressure difference between ice crystals and liquid water around the ice caps, which gives (Scherer and Valenza 2005):

$$P_c - P_l = P_A + \gamma_{cl}\kappa_{cl}^s = P_{\Delta\rho} + P_f \tag{1}$$

where, P_c is the pressure of ice tips (Pa), P_l the pressure of surrounded liquid phase (Pa), $P_{\Delta\rho}$ and P_f are the pressures induced by respectively density change and energy change when water solidifies: $P_{\Delta\rho} = (V_l / V_c - 1)(P_l - P_e)$ and $P_f = S_f(T_0 - T) + C_f\left[(T - T_0 + T\ln(T_0/T))\right]$ with V_c the molar volume of ice crystal (m^3/mol), V_l the molar volume of liquid phase (m^3/mol), S_f the melting entropy related pressure term at a reference state (Pa/K), C_f the heat capacity change related pressure term as ice forms at current temperature T (Pa/K), R the ideal gas constant (J/mol/K), T_0 the equilibrium bulk freezing/melting temperature (K). Due to the different functions of the energy change, the present energy related pressure term is slightly different with the general internal frost case for pure water saturated CBPMs shown elsewhere (Dai *et al*. 2013, Scherer and Valenza 2005). It is noteworthy that, $P_{\Delta\rho} < 0$ as $P_l > P_e$, because $V_c > V_l$. This indicates that raising liquid pressure tends to melt ice. For the energy related term P_f, $S_f(T_0 - T) >> C_f\left[(T - T_0 + T\ln(T_0/T))\right]$, in many cases, P_f reduces to a simpler expression, $P_f = S_f(T_0 - T)$ with $S_f \approx 1.2$ MPa/K.

UNFROZEN LIQUID-LIKE LAYER

The unfrozen liquid-like layer (ULLL) on the surface of ice has been observed more than 150 years. There are three proposed mechanisms for the formation of this layer: pressure melting, frictional heating, and intrinsic premelting (Dash *et al*. 1995). The thickness of this layer, which is reported to be ranging from one to three molecular layers, depends preliminary on the temperature. The requirement of minimal Helmholtz free energy (or Gibbs free energy instead when the work by pressure is negligible) in equilibrium helps to link the thickness of ULLL to the classic thermodynamic properties of water--ice system (Zeng 2012),

$$\frac{\Delta H(T_0 - T)}{T_0 V_c} = \frac{\Delta\gamma\partial F}{\partial\delta} \tag{2}$$

where ΔH is the fusion enthalpy (J/mol), $\Delta\gamma$ is the surface energy differences as ice premelts (N/m), F is the specific interfacial potential (-). Once the term $\partial F/\partial\delta$ is determined, the relationship between the thickness of ULLL and the temperature can be evaluated specifically. In addition, the choice of $F(\delta)$ depends on the surface force acting between the solid-liquid and the liquid-ice interfaces for ice growing in fine pores (Dash *et al.* 1995). For an exponentially distributing force between the two interfaces, $F=\exp(-2\delta/\varepsilon)$ (Petrov and Furo 2009), the thickness of ULLL can be expressed as,

$$\delta=\frac{-\varepsilon}{2}\ln\left[\frac{-\varepsilon\Delta H(T_0-T)}{2T_0V_c\Delta\gamma}\right] \tag{3}$$

where ε is a parameter that can be determined by experiments. If van der Waals forces were considered, where the repulsive dispersion force between two microscopic bodies is in a limiting separation σ, $F(\delta)=\delta^2/(\delta^2+\sigma^2)$ and $\delta>>\sigma$ was adopted in general case, the thickness of ULLL is then given by

$$\delta=\left[\frac{-\Delta H(T_0-T)}{2T_0V_c\Delta\gamma\sigma^2}\right]^{-1/3} \tag{4}$$

In fact, Eqs. (3) and (4) capture the well-used semi-empirical models for estimating the thickness of ULLL between ice and pore wall,

$$\delta\propto\ln(T_0-T) \tag{5a}$$

$$\delta\propto(T_0-T)^{-1/3} \tag{5b}$$

Generally, Eq. (5a) maybe suitable to describe the thickness of ULLL when ice is exposed to air, whereas Eq.(5b) was argued to capture the thickness of ULLL when ice is in contact with rough solid surface (Dash *et al.* 1995). Furthermore, Eq.(5b) was adopted widely in engineering application, e.g., estimation of pore size distribution (PSD) by differential scanning calorimetry (DSC) with the ULLL correction (Table 1) (Fagerlund 1973). Recent study by Petrov and Furo (2009) suggested that the thickness of ULLL with temperature obeys Eq.(5a) (Table 1), and is much thinner than that used in (Fagerlund 1973).

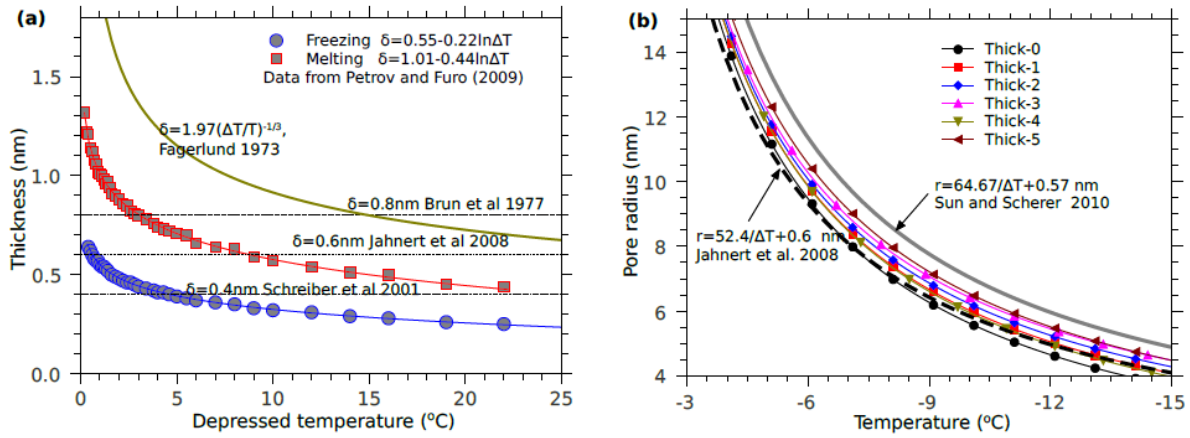

Figure 2 (a), Thickness of unfrozen liquid-like layer between ice and pore wall (Data from (Schreiber *et al*. 2001, Brun *et al*. 1977, Fagerlund 1973, Petrov and Furo 2009, Jahnert *et al*. 2008}), and (b), Gibbs-Thompson relationship corrected by the different ULLL values and those well used in the literature (Sun and Scherer 2010b, Jahnert *et al*. 2008).

Table 1 Thickness of unfrozen liquid-like layer used in the present study

Name	Value (nm)	Method	Ref.
Thick-1	$\delta=0.4$	DSC measurement	Schreiber *et al*. 2001
Thick-2	$\delta=0.6$	DSC measurement	Jahnert *et al*. 2008
Thick-3	$\delta=0.8$	DSC measurement	Brun *et al*. 1977
Thick-4	$\delta=0.55-0.22\ln(\Delta T)$	Theoretical calculation	Petrov and Furo 2009
Thick-4	$\delta=01.97\lvert\Delta T\rvert^{-1/3}$	Theoretical calculation	Fagerlund 1973

Some DSC measurements suggested that the thickness of ULLL is a constant value below 1 nm, e.g., 0.4 nm (Schreiber *et al*. 2001), 0.6 nm (Jahnert *et al*. 2008) and 0.8 nm (Brun *et al*. 1977), see also Table 1. The values and models for the thickness of ULLL mentioned above are also displayed in Figure 2(a) for comparison. The thickness of ULLL by the model of Thick-5, i.e., $\delta=01.97|\Delta T|^{-1/3}$ nm approaches the constant value of Thick-3

(0.6 nm) as $\Delta T = 35$℃. Note that the thickness of ULLL by the model of Thick-4 arrives 0.3 nm when $\Delta T = 10$℃, around one molecular layer of water.

Thermodynamic descriptions of the solid/liquid phase transition in confined geometries predict a shift of the freezing or melting temperature in a function of the pore width, named Gibbs--Thomson equation. For a pure substance in a cylindrical pore of radius R, it gives,

$$\Delta T = \frac{2\gamma_{lc}}{S_f\left(R-\delta\right)} \text{ or } R = \frac{2\gamma_{lc}}{S_f \Delta T} + \delta \tag{6}$$

This expression suggests the presence of a noncrystallized water layer of width δ in coexistence with the confined ice just below depressed temperature ΔT. Figure 2(b) shows the Gibbs-Thomson curves by the different ULLL models. Under a certain subzero temperature, thickening the ULLL tends to enlarge the pore radius. This effect is significant for nano pores (Jahnert *et al*. 2008, Han *et al*. 2012). Figure 2(b) also displays the Gibbs-Thomson curves with different thermodynamic parameters in the literature (Sun and Scherer 2010b, Jahnert *et al*. 2008).

POROELASTICITY

Understanding the physical--chemical process of freezing of water confined in thin pores helps to investigate the pressures building up during freezing, which in turn affects the pores and solid substrates. This, however, remains difficult to associate the local (maybe micro) pressures to macro measurements (e.g., linear or volumetric deformation). Poroelastic analysis can be a good approach to bridge the local phase changes inside pores with the macro deformation of porous material (Coussy 2005, 2010). For simplification, we assume that a porous material is free to expand or shrink ($\Sigma = 0$), the total strain (ε) of the material is thus composed of the terms by internal stresses (pore pressures) and by pure thermal effect,

$$\varepsilon = \frac{1}{3}\frac{b_c P_c + b_l P_l}{K} + \alpha_s\left(T - T_0\right) \tag{7}$$

where K is the bulk modulus of porous material (GPa), α_s the apparent TEC of solid phases (1/℃), b_c the Biot coefficient of ice crystals and b_l the Biot coefficient of liquid water (-). Note that Eq.(7) has minor differences with the expression in (Sun and Scherer 2010a, Wang *et al*. 2014), where the ice pressure P_c was replaced by the crystallization pressure P_A and a pore shape parameter was introduced to interpret the total strain. In this study, the pore shape interpretation was neglected due to the lack of available data.

The deformation of porous skeleton, together with the pore pressures of the phases and TEC discrepancies between the pore fluids and the solid substrate, in turn affects the porosity. This yields,

$$\varphi_{J=cl} = 3b_J\varepsilon + \frac{P_J}{N_{JJ}} - 3\alpha_{\phi J}\left(T - T_0\right) \tag{8}$$

where φ_J is the deviation of the partial porosity occupied by phase J (-), N_{JJ} the Biot's coupling modulus (Pa), $\alpha_{\phi J}$ the coupling TEC of phase J (1/℃). Statistically, a CBPM can be treated as an isotropic material in an appropriate scale. This helps to evaluate the parameters as follows (Coussy 2005,2010),

$$b = 1 - \frac{K}{K_s}, b_{J=c,l} = bs_J, \frac{1}{N_{JJ}} = \frac{b_J - \phi s_J}{K_s}, a_{\phi J} = \alpha_s\left(b_J - \phi_0 s_J\right) \tag{9}$$

where b is the apparent Biot coefficient (-), K_s the bulk modulus of solid matrix (GPa). Under sealed (undrained) freezing condition, the mass conservation of total pore liquid currently contained in the porous materials allows relation of the liquid pressure P_l to the saturation degree s_l and the environmental temperature T, see Refs. (Zeng *et al*. 2013a, 2014a) for more details. Further analysis by considering the local pressure difference between ice crystals and liquid water around the ice caps (Eq.(1)) and the constitutive equation for micro local pore pressure and macro strain (Eq.(7)) finally gives,

$$P = P_{\Delta\rho} + P_{\Delta H} + P_{\Delta\alpha} \tag{10a}$$

$$\varepsilon = \varepsilon_{\Delta\rho} + \varepsilon_{\Delta H} + \varepsilon_{th} \tag{10b}$$

where the subscripts $\Delta\rho$, ΔH and $\Delta\alpha$ denote the effects of density change, enthalpy change and TEC discrepancy between pore fluids and solid matrix. It is noteworthy that, in Eq. (10), ε_{th} not only captures the hydrothermal strain induced by the TEC discrepancies between the pore fluids and the solid substrate, but also that of the pure thermal expansion/contraction of the solid phases as temperature increases/decreases. The detailed expressions for the specific terms in Eq. (10) are displayed in Table 2, where B, P_s, $\mathcal{T}_S$ and $\mathcal{T}_\alpha$ are the coefficients: $B = b_c V_l / V_c + b_l$, $\mathrm{T}_s = \rho_l^0\left(Bb_c / K + s_c\phi_0 / K_c + 1/N_{cc}\right)$, $\mathcal{T}_\alpha = 3\left[\rho_l^0\left(\alpha_s - \alpha_{\phi l} - S_l\alpha_l\right) + \rho_c^0\left(\alpha_s - \alpha_{\phi c} - S_c\alpha_c\right)\right]$ and

$\mathrm{P}_s = \rho_l^0\left(s_l\phi_0 / K_l + Bb_l / K + 1/N_{ll}\right) + \rho_c^0\left[Bb_l / K + \left(s_c\phi_0 / K_c + 1/N_{cc}\right)V_l / V\right]$, with ϕ_0 and ρ_J^0 are the initial porosity (-) and density of phase J ($\mathrm{kg/m^3}$). The detailed derivation of Eq. (10) can be found in (Zeng *et al*. 2013a,2014a).

Table 2 Specific expressions for the terms in Eq.(10)

Pressure	Strain	Note
$P_{\Delta\rho} = -\phi_0\Delta\rho s_c / \mathrm{P}_s$	$\varepsilon_{\Delta\rho} = -B\phi_0\Delta\rho s_c / (3K\mathrm{P}_s)$	Density change
$P_{\Delta H} = \left(b_c / B - \mathrm{T}_s / \mathrm{P}_s\right) / P_f$	$P_{\Delta H} = \left(b_c\mathrm{P}_s - B\mathrm{T}_s\right)P_f / (3K\mathrm{P}_s)$	Enthalpy change
$P_{\Delta\alpha} = -\mathrm{T}_\alpha\left(T - T_0\right) / \mathrm{P}_s$	$\varepsilon_{\Delta\alpha} = \left[\alpha_s - B\mathrm{T}_\alpha / (K\mathrm{P}_s)\right]\left(T - T_0\right)$	Thermal effect

ANALYSIS AND DISCUSION

Ice volume distribution

When evaluating pressures and strains of a CBPM, one should first determine the water saturation degree s_l or ice saturation degree s_c that is directly associated with the thickness of ULLL and PSD. Generally the water saturation degree s_l can be evaluated by experimental measurements, e.g., the DSC measurement for mortars in (Sun and Scherer 2010b), or by indirect method based on PSD of the material determined by other methods, e.g., mercury intrusion porosimetry (MIP) (Fabbri *et al*. 2013, Zeng *et al*. 2014b). In the present study, we employed the indirect method to estimate the IVD and water saturation degree with temperature. The principle of the indirect estimation method relies on the similar physical processes of ice penetration under freezing and mercury intrusion under pressure: a non-wetting phase (ice or mercury) invades pore structure progressively and a complementary wetting phase (pore water or air) retreats correspondingly (Zeng *et al*. 2014b). Figure 3 shows a typical PSD of a hardened cement paste (HCP) specimen (w/c=0.5) (Zeng *et al*. 2014a), where the pores are mainly distributed in the regions of 3--100 nm. For modeling purpose, a multi-peak Gauss formula was used to fit the MIP PSD curve. Excellent agreements between the multi-peak Gauss fitting and experimental data were found in Figure 3.

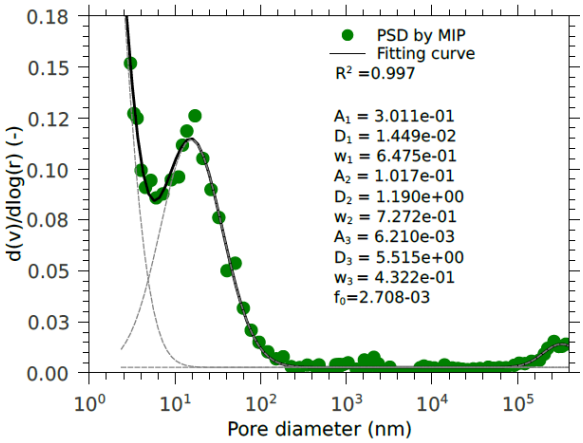

Figure 3 Pore size distribution of a HCP with multi-peak Gauss fitting (Data from Zeng *et al*. 2014a)

Considering the contribution of the ULLL, we established a model to evaluate the IVD and water saturation degree with temperature under thermodynamic equilibrium, see (Zeng *et al*. 2014a,b) for more details. Figure 4 shows the differential and cumulative IVDs with temperature for the HCP specimen with the different ULLL models. The very first differential IVD peaks around 0 ℃ in Figure 4(a) can be observed due to the instantaneous ice formation in big capillary pores. The used temperature step is about 0.1 ℃, so the corresponding instantaneous freezing pore size ranges are estimated as $R > 340$ nm according to the Gibbs-Thomson equation. In such large pores, the effect of ULLL is negligible. As temperature decreases, thinner pores are frozen. The second differential IVD peaks appear around -3.7 ℃ without ULLL correction (Thick-0, $\delta = 0$ nm), and around -3.4℃ with the ULLL model of Thick-5, owning to freezing of water confined in the pores of 15 nm (Figure 3). The ULLL effect is significant. For example, the intensity of the differential IVD peak with the ULLL model of Thick-0 (0.986 μl/g) is significantly higher than that with the ULLL model of Thick-5 (0.720 μl/g). The cumulative IVD values, however, show almost the same numbers (Figure 4(b)) because the volumes of the pores $R > 15$ nm remain minor (0.03 ml/g by MIP). As freezing goes on, water in nano pores solidifies. Different ULLL models lead to different IVD results, at -35℃, the values of cumulative

IVD with the ULLL models of Thick-1, 2, 3, 4, and 5 respectively are 0.107, 0.097, 0.088, 0.114 and 0.085 ml/g (Figure 4(b)), heavily lower than those without ULLL correction and the MIP data.

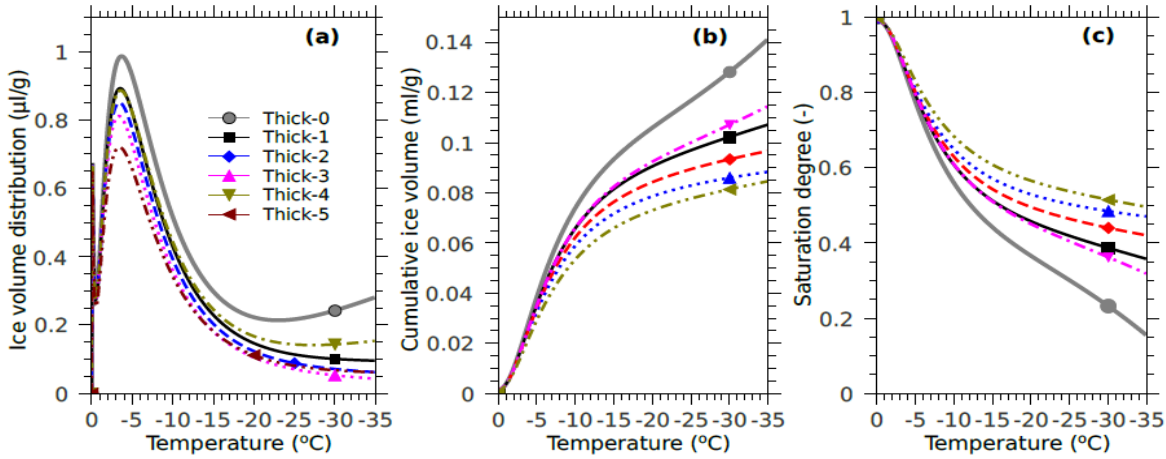

Figure 4 (a) Differential and (b) cumulative ice volume distribution, and (c) water saturation degree versus temperature for the HCP specimen with different ULLL models.

Figure 4(c) displays the water saturation degree s_l upon cooling corrected with the ULLL models. As seen, the values of s_l without ULLL correction always lay below those interpreted with the ULLL models, and thickening the ULLL elevates the s_l values under a subzero temperature. For the non-ULLL case (Thick-0), the entire freezable pores ($R > 1.44$ nm) are occupied by the ice when the temperature decreases to -35 ℃, leaving the water confined in the very tiny gel pores (residual unfrozen volume of 15.6%). When the ULLL is considered, the equilibrium pore radius at -35 ℃ can be changed, e.g., to 1.84, 2.04, 2.24, 1.65 and 2.05 nm for the Thick-1, -2, -3, -4, and -5 models. At the same subzero temperature, consequentially, the unfrozen water occupies more total pores volumes (e.g., around 50% of the total pore volume for the Thick-5 model).

Freezing pressure

Freezing pressures, as decoupled in three different terms in Eq. (10), depend directly on the water/ice saturation degree, temperature and properties of the material and pore fluids. During modeling, we adopted the required parameters of the HCP specimen and pore fluids as follows (Coussy and Monteiro 2008, Zeng *et al*. 2014a,b): $\phi_0 = 0.26$, $K_s = 25.8$ GPa, $K = (1-\phi_0)^2 = 14.1$ GPa, $K_l = 1.8$ GPa, $K_l = 7.8$ GPa, $\alpha_s = 17\times10^{-6}$ 1/K, $\alpha_l = -96\times10^{-6}$ 1/K, $\alpha_c = 52\times10^{-6}$ 1/K. Figure 5(a) shows the pore pressure generated by the density change as ice crystallizes in the pores. The values of pore pressure can be raised up to the magnitude of 100 MPa, consistence with the results reported in (Coussy and Monteiro 2008). However, one should note that in (Coussy and Monteiro 2008) the authors did not consider the effect of ULLL and the lowest freezing temperature was -20 ℃. The values remain significantly lower than those estimated by the classic Clapeyron equation ($P \approx 13.6\times\Delta T \approx 470$ MPa, $\Delta T = 35$ ℃), because we have considered the deformation effects of the porous HCP specimen and pore fluids, see also (Zeng *et al*. 2013). In contrary to the water saturation degree, the values of $P_{\Delta\rho}$ without ULLL correction always lay over those with the ULLL models. In addition, increasing the thickness of ULLL depresses the $P_{\Delta\rho}$ at a subzero temperature. As illustrated in Figure 5(a), at -35 ℃, the values of $P_{\Delta\rho}$ with the ULLL models of Thick-1, 2, 3, 4, and 5 respectively are 138, 117, 103, 152 and 96 MPa, heavily lower than those without ULLL correction (225 MPa). Figure 5(b) displays the curves of $P_{\Delta H}$ that is generated by the energy change of ice formation upon freezing by the different ULLL models. While $P_{\Delta H}$ shows the similar tendency with $P_{\Delta\rho}$, the values of $P_{\Delta H}$ are systematically and dramatically lower than those of $P_{\Delta\rho}$. In addition, $P_{\Delta H}$ almost increases linearly with temperature decreasing for all the ULLL models, because $P_{\Delta H} \propto P_f$ and $P_f \propto \Delta T$ ($P_f \approx 1.2\times\Delta T = 42$ MPa, $\Delta T = 35$ ℃). Again, lowering the thickness of ULLL increases $P_{\Delta H}$, because more heat releases as ice forms in the pores with thinner ULLL.

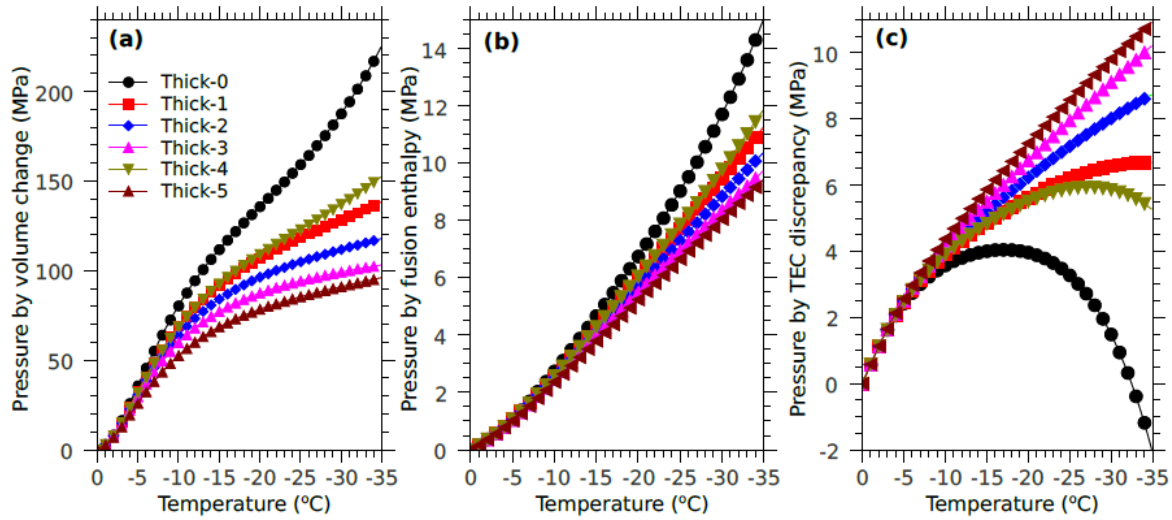

Figure 5 Internal pressures induced by (a) density change, (b) fusion enthalpy, and (c) TEC discrepancy versus temperature for the HCP specimen with different ULLL models

Figure 5(c) presents the curves of hydrothermal stress (or thermal pressure) $P_{\Delta\alpha}$ that is induced by the TEC discrepancies between the pore fluids and solid substrate upon freezing by the different ULLL models. Unlike the values of $P_{\Delta\rho}$ and $P_{\Delta H}$ that increase monotonously with temperature decreasing, the $P_{\Delta\alpha}$ data show completely different ways upon freezing for the different ULLL models. Anomalies of $P_{\Delta\alpha}$ with the ULLL models of Thick-0 and 4 are observed, i.e., $P_{\Delta\alpha}$ increases first to a maximum value then decreases. The increases of $P_{\Delta\alpha}$ with temperature decreasing are originated from the negative TEC of supercooled water ($\alpha_l = -96\times10^{-6}$ 1/K) that expanses as temperature is lowered. Meanwhile both the HCP solid and the ice formed in the pores shrink with temperature decreasing. The synthetic effects of the HCP solid, ice and unfrozen water cause the patterns with which the $P_{\Delta\alpha}$ changes. From the term of $P_{\Delta\alpha}$ shown in Table 2, we find that the sign of $P_{\Delta\alpha}$ depends directly on the thermal pressure coefficient $\mathcal{T}_\alpha$. When $\mathcal{T}_\alpha > 0$, $-\partial P_{\Delta\alpha}/\partial T > 0$, which means that the expansion of the supercooled liquid water dominates the thermal pressure. One the contrary, when $\mathcal{T}_\alpha < 0$, $-\partial P_{\Delta\alpha}/\partial T < 0$, indicating that the contraction of the ice confined in the pores leads the thermal pressure. A critical saturation degree for $\mathcal{T}_\alpha$ emerges as expected. Calculation indicates $P_{\Delta\alpha} = 4.05$ MPa at $T = -17.1$ ℃ and $S_l = 0.407$ for the HCP specimen without ULLL correction, and $P_{\Delta\alpha} = 5.94$ MPa at $T = -27.3$ ℃ and $S_l = 0.385$ for that with the ULLL model of Thick-4, see Figure 5(c). The values of $P_{\Delta\alpha}$ with the ULLL models of Thick-1, 2, 3, and 5 increase monotonously with temperature decreasing because $\mathcal{T}_\alpha$ is always larger than 0.

Freezing strain

Material deformation is an important measurement that inflects the mechanical behaviors of the material under loading and/or internal phase changes. Unlike stress or pore pressure that can be hardly measured directly, deformation or strain of a material can be measured with various methods. Figure 6 shows the strains of the HCP specimen under cooling measured by LVDT, where the detailed measurement method and procedures can be found in (Zeng *et al*. 2014b). It can be seen that the material contracts linearly as the temperature decreases to around -7 ℃ because the pore water remains supercooling. After ice nucleating, the HCP specimen expands instantaneously by about 300 μ (Zeng *et al*. 2014b). As cooling continues, the material expands nonlinearly. The freezing expansions can be roughly captured by the poroelastic analysis, see also (Zeng *et al*. 2014a,b). In Figure 6 are displayed the predicted freezing strains with the different ULLL models. It is noteworthy that the freezing kinetics related to supercooling is still beyond the scope of the poroelastic models, so the pure thermal contraction before ice nucleation and the instantaneous shift of the strain at the nucleation point will not be discussed in this study. It can be seen that the strains of the HCP specimen without ULLL correction are dramatically higher than the measured data. As the thickness of ULLL increases, the predicted strain curve shifts to the lower position in the figure, and captures the experimental data to some extent, e.g., the predicted strain curves with the ULLL models of Thick-2, 3 and 5, see Figure6. For the ULLL models of Thick-1 and 5

that have thickness of 0.4 nm in constant and a logarithm equation decaying with the subzero temperature, the deviation of the predicted strains from the measured data are extended.

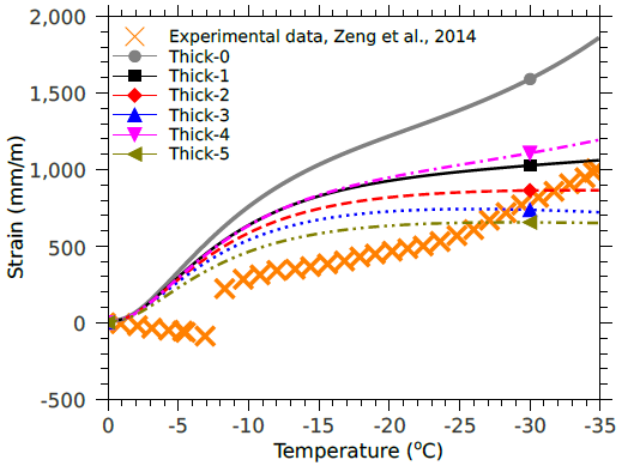

Figure 6 Strains of the HCP specimen under freezing interpreted by different ULLL models and those measured by LVDT (Data from Zeng *et al*. 2014b).

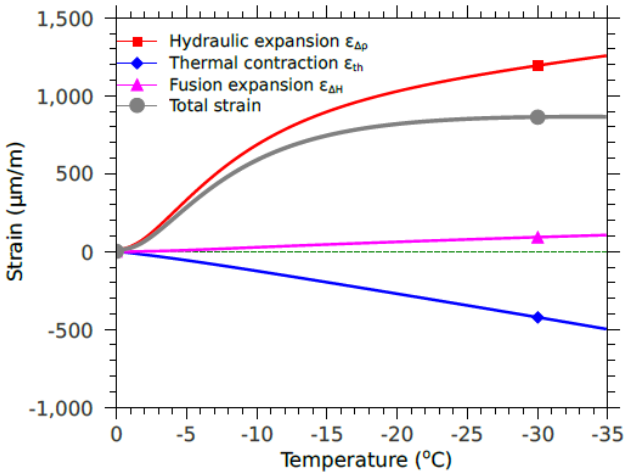

Figure 7 Evolution of the total and specific strains with temperature for the HCP specimen with a constant thickness of ULLL ($\delta = 0.6$ nm)

The origins of the CBPM deformation upon freezing are the effective internal pressure as aforementioned and the pure thermal contraction. More specifically, the total strain of the material is composed of the strains by density change, energy change of water solidification and TEC of the composite system, see Eq. (10). Figure 7 exemplifies the total and the specific strains upon freezing for the HCP specimen with a constant ULLL thickness of 0.6 nm. As seen, the hydraulic expansion $\varepsilon_{\Delta\rho}$, attributed to the hydraulic pressure by the density change as the confined water solidifies, governs the freezing expansion, whereas the fusion expansion $\varepsilon_{\Delta H}$ that is generate from the energy change of ice forming is limited. The thermal strain ε_{th} represents the deformation by pure thermal contraction of the solid paste and that by the hydrothermal stress originated from the TEC discrepancies between the pore fluids and solid substrate as shown in Figure 5(c). While the hydrothermal stress can be as high as 10 MPa, the pure thermal contraction of the HCP specimen remains playing the dominative role on the thermal strain ε_{th}. The coupled effects of the hydrothermal stress and thermal contraction of the solid phases lead to an apparent TEC of 14×10^{-6} 1/K, moderately lower that the TEC of the solid substrate of 17×10^{-6} 1/K.

Note that the matches between the poroelastic models and the experimental data remain coarse, because it has some limitations in the present study that considers an ULLL between pore wall and ice during freezing of which the thickness is constant or changes with temperature. Firstly, we assumed that configurational and vibrational properties of nanoconfined water are the same as those of the bulk. This assumption is challenged by

the disordered structure of ice and water by the actions of confinement. For instance, when the pore size is typically around 3 nm diameter, water freezes to cubic ice, not to the lower energy hexagonal ice, or freezes to a mixture of the two ices with a persistent different structure, thus indicating that crystals and melt coexist. In addition, it have been evidenced that the thermodynamic properties of water vary with both its position in a nanopore and the amount of water in the pore (Han *et al*. 2012, Jelassi *et al*. 2011). Secondly, the properties of pore wall are complex. We assumed a uniform hydrophilic surface for the pores of the CBPM. This assumption maybe too coarse to capture the hydrophilicity of the surfaces of the CBPMs, which are composed of multi hydrates and have extremely complex microstructures (Zeng *et al*. 2012, 2013b). The third limitation of the method used in the present study is the assumption of the cylindrical pores for the cement-based specimens. Porometry measurements by multi methods indicated that pores of CBPMs are much more complex than the simple pores shapes (sphere or cylinder) (Zeng *et al*. 2012). The interactions between the pores wall and water and/or ice molecules, together with the upscaling method (poroelastic approach), provide further research incentives in the future.

CONCLUSIONS

Unfrozen liquid-like layer (ULLL) exists between ice and pore wall due to the mechanisms of pressure melting, frictional heating, and intrinsic premelting. The requirement of minimal Helmholtz free energy with an appropriate specific interfacial potential deduces the well-used semi-empirical models for estimating the thickness of ULLL between the ice crystals and pore wall: $\delta \propto \ln(\Delta T)$ and $\delta \propto (\Delta T)^{-1/3}$.

Five different models for the thickness of ULLL are adopted in this study to interpret the Gibbs-Thomson equation. Analysis results indicate that thickening the ULLL tends to enlarge the equilibrium pore radius under a certain subzero temperature.

Poroelastic model is established to associate the local pore pressure induced by water solidification that takes place in thin pores with the macro material deformation. Both the pore pressure and material strain are composed of the density change, energy change and thermal effect upon freezing.

A typical hardened cement paste (w/c=0.5) with multi-peak pore size distribution is used in the study. The modeling results indicate that the ULLL affects the ice volume distribution and water saturation degree. Without the ULLL correction, it may overestimate the ice volume and underestimate the water saturation degree under a subzero temperature.

Raising the thickness of ULLL tends to lower the pore pressures by density change and energy change as water solidifies, but increase the hydrothermal pressure by TEC discrepancies between pore fluids and solid substrate. Anomalies of hydrothermal pressure emerge for the cases without ULLL correction and with a very thin ULLL attributed to the negative TEC of the supercooled water.

The appropriate ULLL correction mitigates the deviation between the predicted freezing strains and the measured data. More rigorous studies on the interactions between the pores wall and water and/or ice molecules, together with the upscaling method, are required in the future.

ACKNOWLEDGMENTS

The research is sponsored by the National Natural Science Foundation of China (No.51408536).

REFERENCES

Brun, M., Lallemand, A., Quinson, J.F. and Eyraud, C. (1977) “A new method for the simultaneous determination of the size and the shape of pores: the thermoporometry”, *Thermochim. Acta*, 21, 59-88.

Coussy, O. (2005) “Poromechanics of freezing materials”, *J Mech Phys Solids*, 53, 1689-1718.

Coussy, O. (2010) *Mechanics and physics of porous solids*. John Wiley & Sons Ltd.

Coussy, O., and Monteiro, P.J.M. (2008) “Poroelastic model for concrete exposed to freezing temperature”, *Cem Concr Res*, 38, 40-48.

Dai, Q., Ng, K., Liu, Y. and Yu, X. (2013) “Investigation of internal frost damage in concrete with thermodynamic analysis, microdamage modeling, and time-domain reflectometry sensor measurements, *J Mater Civil Eng*, 25, 1248-1259.

Dash, J.G., Fu, H. and Wettlaufer, J.S. (1995) “The premelting of ice and its environmental consequences”, *Rep Progr Phys*, 58, 115-167.

Fabbri, A. and Fen-Chong, T. (2013) “Indirect measurement of the ice content curve of partially frozen cement based materials”, *Cold Reg Sci Technol*, 90-91, 14--21.
Fagerlund, G (1973) “Determination of pore-size distribution from freezing-point depression”, *Mater Struct,* 6, 215--225.
Han, Y.Y., Shuai, J., Lu, H.M. and Meng, X.M. (2012) “Size- and dimensionality-dependent thermodynamic properties of ice nanocrystals”, *J Phys Chem B*, 116, 1651--1654.
Jahnert, S, Vaca Chavez, F., Schaumann, G.E., Schreiber, A., Schonhoff, M. and Findenegg, G.H. (2008) “Melting and freezing of water in cylindrical silica nanopores, *Phys Chem Chem Phys*, 10, 6039--6051.
Jelassi, J., Castricum, H.L., Bellissent-Funel, M.C., Dore, J., Webber, J.B.W. and Sridi-Dorbez, R. (2010) “Studies of water and ice in hydrophilic and hydrophobic mesoporous silicas: pore characterisation and phase transformations”, *Phys Chem Chem Phys*, 12, 2838--2849.
Petrov, O. and Furo, I (2009) “NMR cryoporometry: Principles, applications and potential”, *Prog Nucl Mag Sp*, 54, 97--122.
Scherer, G. (1999) “Crystallization in pores”, *Cem Concr Res*, 29, 1347--1358.
Scherer, G. and Valenza, J. “Mechanisms of frost damage”. In: J. Skalny, F. Young (Eds.), *Materials Science of Concrete VII*. *American Ceramic Society*, 2005, pp.209--246.
Schreiber, A., Ketelsen, I. and Findenegg, G.H. (2001) “Melting and freezing of water in ordered mesoporous silica materials”, *Phys Chem Chem Phys,* 3, 1185--1195.
Sun, Z. and Scherer, G. (2010a) “Effect of air voids on salt scaling and internal freezing”, *Cem Concr Res*, 40, 260--270.
Sun, Z. and Scherer, G. (2010b) “Pore size and shape in mortar by Themoporosimetry”, *Cem Concr Res,* 40, 740--751.
Wang, Z., Zeng, Q., Wu, Y., Wang, L., Yao, Y. And Li, K. (2014) “Relative humidity and deterioration of concrete under freeze--thaw load”, *Constr Build Mater*, 62, 18--27.
Zeng, Q., Fen-Chong, T., Dangla, P. and Li, K. (2011) “A study of freezing behavior of cementitious materials by poromechanical approach”, *Int J Solid Struc*, 48, 3267--3273.
Zeng, Q. (2012) *Poromechanical Behavior of Cement-Based Materials Subjected to Freeze--Thaw Actions with Salts: Modelling and Experiments*. (PhD Thesis) Universie Paris-Est, France, 2012.
Zeng, Q., Li, L., Fen-Chong, T. and Dangla, P. (2012) “Pore structure characterization of cement pastes blended with high-volume fly-ash”, *Cem Concr Res*, 42, 194--204.
Zeng, Q., Li., K. and Fen-Chong, T. (2013a) “Elastic behavior of saturated porous materials under undrained freezing”, *Acta Mech Sinica*, 29, 827--835.
Zeng, Q., Luo, M., Pang, X., Li, L. and Li, K. (2013b) “Surface fractal dimension: An indicator to characterize the microstructure of cement-based porous materials”, *Appl Surf Sci*, 282, 302--307.
Zeng, Q., Li, L., Pang, X., Gui, Q. and Li, K. (2014a) “Freeze--thaw behavior of air entrained cement paste saturated with 10wt.\% NaCl solution”, *Cold Reg Sci Technol*, 102, 21--31.
Zeng, Q., Fen-Chong, T. and Li, K. (2014b) “Freezing behavior of cement pastes saturated with NaCl solution”, *Constr Build Mater,* 59, 99--110.